

1
2 **Permafrost changes in the northwestern Da Xing'anling**
3 **Mountains, Northeast China in the past decade**

4 Xiaoli Chang ^{1,2*}, Huijun Jin^{2,3*}, Ruixia He ², Yanlin Zhang ¹, Xiaoying Li ⁴, Xiaoying
5 Jin ² and Guoyu Li ²

6 ¹School of Earth Science and Spatial Information Engineering, Hunan University of Science and
7 Technology, Xiangtan, Hunan 411201, China,

8 ²State Key Laboratory of Frozen Soils Engineering, Northwest Institute of Eco-Environment and
9 Resources, Chinese Academy of Sciences, Lanzhou 730000, China,

10 ³School of Civil Engineering, Institute of Cold-Regions Science and Engineering, and Northeast-China
11 Observatory and Research-Station of Permafrost Geo-Environment (Ministry of Education), Northeast
12 Forestry University, Harbin 150040, China,

13 ⁴Key Laboratory of Sustainable Forest Ecosystem Management (Ministry of Education) and College of
14 Forestry, Northeast Forestry University, Harbin 150040, China

15 *These authors contributed equally to this work.

16 *Correspondence to:* R. He: ruixiahe@lzb.ac.cn

17
18 **Abstract.** Under a pronounced climate warming, permafrost has been degrading in most areas, but it
19 is still unclear in the northwestern part of the Da Xing'anling Mountains, Northeast China. According to
20 a ten-year observation of permafrost and active-layer temperatures, the multi-year average of mean
21 annual ground temperatures at 20 m was -2.83 , -0.94 , -0.80 , -0.70 , -0.60 and -0.49 °C, respectively,
22 at Boreholes Gen'he4 (GH4), Mangui3 (MG3), Mangui1 (MG1), Mangui2 (MG2), Gen'he5 (GH5) and
23 Yituli'he2 (YTLH2), with the depths of permafrost table varying from 1.1 to 7.0 m. Ground cooling at
24 shallow depths has been detected, resulting in declining thaw depths in Yituli'he during 2009-2020,
25 possibly due to relatively stable mean positive air temperature and declining snow cover and dwindling
26 local population. In most study areas (e.g., Mangui and Gen'he), permafrost warming is particularly
27 pronounced at larger depths (even at 80 m). These results can provide important information for regional
28 development and engineering design and maintenance, and also provide a long-term ground temperature
29 dataset for the validation of models relevant to the thermal dynamics of permafrost in Da Xing'anling
30 Mountains. All of the datasets are published through the National Tibetan Plateau Data Center (TPDC),
31 and the link is <https://doi.org/10.11888/Geocry.tpd.271752> (Chang X, 2021).

32 **1 Introduction**

33 Permafrost, defined as ground that remains at or below 0 °C consecutively for two or more years, is
34 widespread in high-latitude and high-elevation regions (Zhang et al., 2007). One quarter of the Northern
35 Hemisphere and 17% of the Earth's currently exposed land surface are underlain by permafrost (Gruber,
36 2012). Areal extent of permafrost in China is estimated at about 1.59×10^6 km² (Youhua et al., 2012),
37 mainly on the Qinghai-Tibet Plateau (about 1.06 - 1.17×10^6 km²) (Zou et al., 2017; Cao et al., 2019), in
38 northeastern China (about 3.1×10^5 km²) (Zhang et al., 2021) and mountainous areas in northwestern
39 China (Cao et al., 2018). Northern part of Northeast China is also characterized by the extensive and
40 stable inversion of air temperature in winter, thick surficial deposits, dense vegetation, extensive snow
41 cover, and widespread distribution of wetlands in valley bottoms and lowlands, resulting in strong
42 regional differentiations in permafrost features (Jin et al., 2007). Therefore, the latitudinal permafrost in
43 Northeast China is referred to as the "Xing'an (Hinggan)-Baikal permafrost (XBP)" (Jin et al., 2007), a
44 distinct type of ecosystem-dominated permafrost (Shur and Jorgenson, 2007).

45 Permafrost is sensitive to climate change (Farquharson et al., 2019; Sim et al., 2021; Zhang et al., 2019;
46 Ran et al., 2018) and surface disturbances (Guo et al., 2018; Li et al., 2019; Li et al., 2021). It has
47 experienced significant warming and widespread degradation during the last several decades (Jin et al.,
48 2000; Jin et al., 2007; Zhang et al., 2019; Jin et al., 2021; Chen et al., 2020), evidenced by deeper seasonal
49 thaw (Luo et al., 2018), thinning and warming permafrost (Gruber, 2012; Jin et al., 2021; Jin et al., 2007;
50 Romanovsky et al., 2010), and an areal reduction of permafrost in northeastern China (Li et al., 2021;
51 Zhang et al., 2021). The permafrost change has attracted extensive attention worldwide (Biskaborn et al.,
52 2019), because it has significant potential impacts on the terrestrial eco-hydrological processes (Zhang
53 et al., 2017; Schuur and Mack, 2018; Zhang et al., 2018a; Ala-Aho et al., 2021; Ran et al., 2022) and
54 carbon cycling (Mu et al., 2020; Schuur et al., 2015). In recent decades, huge efforts have been dedicated
55 to developing physically based models to reproduce and predict the thermal dynamic processes of
56 permafrost and their influences. However, lacking long term and systematic in-situ observation of
57 permafrost temperature is an apparent bottleneck for the mentioned relevant analysis and model
58 calibration or validation. The observation in deep ground is especially rare and precious.

59 As a main distribution region of high latitudes permafrost in China, the intensity and progress on
60 permafrost observation in Da Xing'anling Mountains area was falling far behind other permafrost

61 regions, e.g., the Qinghai-Tibetan Plateau. Most of such investigation and observation in Da Xing'anling
62 mountains area were aimed at serving some specific short term projects in economic development,
63 engineering design and construction, e.g., road construction and coalmining (Jin et al., 2007), and they
64 were terminated upon the project completion. In recent years, numerous local studies on permafrost
65 change have been carried out. However, most of them have been based on air and/or ground surface
66 temperatures provided by weather stations, reanalysis data (Wei et al., 2011; Zhang et al., 2018b; Zhang
67 et al., 2021), or short-term ground thermal observations (He et al., 2021; Jin et al., 2007). Thus, it is hard
68 to more accurately feature and evaluate the latest distribution and future changes of permafrost in
69 Northeast China under the combined influences of warming climate and human activities (Serban et al.,
70 2021). Similar to the Circumpolar Active Layer Monitoring (CALM) sites (Brown et al., 2000; Grebenets
71 et al., 2021; Shiklomanov et al., 2012), or CALM-South sites (Guglielmin, 2006; Guglielmin et al., 2012;
72 Hrbáček et al., 2021), a comprehensive observing system was gradually established since 2009 at Gen'he
73 (GH), Yituli'he (YTLH), and Mangui (MG) in the northwestern part of the Da Xing'anling Mountains,
74 Northeast China. Periodical collection and calibration of data on the thermal regimes of soils in the active
75 layer and permafrost at depths have been carried out in boreholes, generally reaching 20 m in depth and
76 one of them, 80 m. This thus presents an opportunity to observe the thermal characteristics of the XAP
77 at depths and to understand and evaluate temporal changes in permafrost features in different landscapes
78 under a warming climate. These results can provide important information for regional planning,
79 development, and engineering design and maintenance in Northeast China. It can also provide a long-
80 term ground temperature dataset for the validation of models relevant to the thermal dynamics of
81 permafrost in Da Xing'anling Mountains.

82 **2 Study area**

83 The Gen'he Station of China Forest Ecological Research Network (CFERN), Yituli'he Permafrost
84 Observatory (YPO), and Mangui Permafrost Station (MPS) are found in the discontinuous permafrost
85 zone of Northeast China (Figure 1), where it is characterized by a cold temperate continental climate
86 under the influences of alternating monsoons. Multi-year averages of mean annual air temperature
87 (MAAT) were $-4.0\text{ }^{\circ}\text{C}$ at Gen'he (1961–2020), $-5.2\text{ }^{\circ}\text{C}$ at the YPO (1965–2005) and $-5.8\text{ }^{\circ}\text{C}$ at the MPS
88 (1996–2005). In the same periods, the multi-year average of annual precipitation was 440 mm at Gen'he,

89 460 mm at the YPO, and 480 mm at the MPS. Annual precipitation falls concentratively in the form of
90 summer rain, according to the chorographic record of Gen'he city. Snowfall (snow water equivalent, or
91 SWE) accounts for about 12~20% of annual total precipitation. Stable snow cover usually starts to occur
92 on the ground surface in the late October and generally disappears in the next April.

93 Vegetation differs slightly from site to site where Boreholes GH4, GH5, YTLH1, YTLH2, MG1, MG2
94 and MG3 are located (Figure 1 and Table 1). Borehole GH4 is in a larch (*Larix gmelinii*) forest, whereas
95 Boreholes GH5, YTLH1, YTLH2 and MG2 are in sedge (*Carex tato*) meadows. The Borehole MG3 is
96 in an open backyard, and Borehole MG1, in a birch (*Betula*) shrubland with sedges (*Carex tato*) as an
97 understory. However, soil types are similar (brown coniferous forest soil).

98

99 Among the seven boreholes, Borehole YTLH1 of 8.15 m in depth was first installed for monitoring the
100 hydrothermal dynamics of active layer and shallow permafrost at the end of 2008, with weekly manual
101 measurement of soil temperatures since 2009. However, in order to monitor the permafrost temperature
102 at the depth of zero annual amplitude (generally at 10-25 m in Northeast China), an additional borehole
103 (YTLH2) was drilled to a depth of 20 m at a nearby site (10 m away from the YTLH1) with almost
104 identical physical and vegetative conditions on the ground surface. The thermistor cables were
105 permanently installed for manually monitoring ground temperatures since 2010. Boreholes GH4, GH5,
106 MG1, MG2 and MG3 have been monitored since the beginning of 2012, but for different observational
107 frequencies (Table 1). These thermistor cables were assembled by the State Key Laboratory of Frozen
108 Soils Engineering (SKLFSE), Cold and Arid Regions Environmental and Engineering Research Institute
109 (CAREERI; now renamed to the Northwest Institute of Eco-Environment and Resources, or NIEER),
110 Chinese Academy of Sciences (CAS), Lanzhou, China, with an accuracy of ± 0.05 °C in the temperature
111 range from -30 to $+30$ °C, and ± 0.1 °C, from -45 to -30 °C and $+30$ to $+50$ °C.

112 For continuous observation, data for ground temperatures at the Borehole GH4 were automatically
113 collected hourly by the Micrologger CR3000 (USA), whereas at other sites were manually measured
114 with a multi-meter (Fluke 189®). Unfortunately, not all records for soil temperature are complete for all
115 boreholes. For example, there were two hiatuses for the records of Borehole GH4 (2014-2016 and 2017-
116 2019) due to the logger damage. Manual records from January to June in 2014 for other boreholes were
117 lost in mailing. The measurement at MG3 was halted in 2016 because of borehole damage and that at
118 GH5 and YTLH2, in 2020, due to the outbreak of the COVID-19 virus and the ensued traffic control.

119 The specifics are presented in Table 1.

120 **3 Results**

121 **3.1 Ground temperatures in near-surface permafrost and active layer**

122 Ground temperatures of near-surface soil (e.g., at depths of 1 and 2 m) responds quickly to changes in
123 air temperature, but the change patterns of ground temperatures show a reduction of amplitude with
124 increasing depth in all these boreholes. In Boreholes GH4, MG3, YTLH1 and YTLH2, seasonal
125 variations in ground temperature still could be detected at the depth of 5 m. However, at depths of 3 and
126 4 m, variations in winter ground temperatures gradually flattens out in Boreholes GH5, MG1 and MG2,
127 and only the annual variability in summer ground temperatures can be detected at the depth of 5 m (Figure
128 2). Therefore, only a small temperature amplitude (0.5~1.0°C) was detected at the depth of 5 m in
129 comparison with that at 3 m (2~3°C).

130 Based on the thermal observation at Borehole MG1, 2.6 m (2017) and 1.9 m (2020) in depth were
131 respectively the maximum and minimum depths of the permafrost table (Table 2). Combining the data
132 in Figure 2b and other observational data, the active layer thickness (ALT) at Borehole MG2 increased
133 from 4.3 m (2012) to 4.8 m (2016), but thinned to 4.2 m (2019) afterwards. The permafrost table at MG3
134 was located at 2.8 m (2012 and 2013), 4.0 m (2014) and 3.3 m (2015) in depth during the observation
135 period. Subtle freeze-thaw cycles were observed at 2.0 m in depth in Borehole GH4 (Figure 2a₂), and the
136 0 °C isotherms in Figure 3a indicated a range of ALT from 2.2 m (2016) to 2.0 m (2018). In Borehole
137 GH5, despite of a small temperature range (0.5°C) at the depth of 6.0 m, freeze-thaw cycles took place.
138 During the monitoring period, the sensor at 7.0 m in depth showed all negative temperatures, but in the
139 left proximity of 0 °C, all year round, with a multi-year average of mean annual soil temperature at
140 -0.08°C. The thawing front reached down to the depth of 7.0 m every year (Figure 3b), which means the
141 permafrost table here has been lowered to 7.0 m in depth. In Borehole YTLH1, ground thaw occurred
142 occasionally at 2.0 m, for an example, in October 2016, but the ALT mostly varied from 1.5 m (2011) to
143 1.0 m (2017) during the observation (Figure 3c). In the same period in 2016, -0.1 °C was registered as
144 the highest temperature at 2.0 m in depth in Borehole YTLH2 (Figure 2c₂), but an above-zero temperature,
145 at 1.5 m depth. The depth of the permafrost table fluctuated between 1.6 m (2017) and 2.0 m (2011 and
146 2016) (Figure 3d and Table 2).

147 3.2 Change trends of permafrost temperature at depths

148 Figure 4 highlights the changes in thermal regimes of permafrost at different depths in Boreholes MG1,
149 MG2 and MG3. Ground temperature was on the rise, but its amplitude decreased with depth since the
150 beginning of observation in 2012. The depth of zero annual amplitude (ZAA) was estimated to be the
151 place where ground temperature changes by no more than 0.1°C throughout a year (Everdingen, 1998
152 (revised 2005)). Although the ground temperature was not measured periodically with a very fine time
153 step and some values were lost, the estimation could still be reasonable, because the temperature
154 fluctuation in deep ground is significantly dampened. According to the monitoring data, the depth of
155 ZAA varies among different boreholes (Table 2) without considering interannual changes. In order to
156 show more accurate thermal states of permafrost, ground temperatures of 20m were chosen to compare
157 within different boreholes in this paper. In Borehole MG1, the amplitude of ground temperatures below
158 8 m in depth was no more than 0.4 °C, and seasonal variability was hardly detectable at depths of 16 and
159 20 m. The results of linear fitting (red trend lines) indicate an overall warming trend of permafrost during
160 2012-2020. A multi-year average of mean annual ground temperature (MAGT, at 20 m; from 2012 to
161 2020) of -0.77 °C was obtained in Borehole MG1. In Borehole MG2, ground temperature varied slightly
162 (± 0.06 °C) with the seasons even at the depth of 20 m, where the MAGT was about -0.69 °C. Permafrost
163 here was also warming, with a rising amplitude of 0.1~0.2 °C from 2012 to 2020. The valid monitoring
164 period was less than 5 years in Borehole MG3 (1 January 2012 to 29 April 2016), when the largest ground
165 temperature range of 0.2-0.5 °C was detected between 8 m and 20 m. Similar to the Borehole MG2,
166 permafrost at 20 m in depth in Borehole MG3 has been experiencing some seasonal variations, with a
167 multi-year average of MAGT at -0.94 °C (Table 2).

168 Permafrost at depths of 8 and 20 m in Boreholes GH4 and GH5 (Figure 5) warmed by 1.5-0.2 and 0.2-
169 0.1°C, respectively, during 2012-2020. The warming of permafrost at GH5 was insignificant in
170 comparison with that at other sites. Mean annual soil temperature at 8 m in depth have slightly warmed
171 from -0.17 °C in 2012 to -0.16 °C in 2019, and; the MAGT at 20 m in depth, from -0.60 to -0.57 °C
172 over the same period. MAGT at 20 m in depth was averaged at -0.59 °C during 2012-2019. However,
173 permafrost at GH4 was relatively cold, with a multi-year average of MAGT at -2.84 °C at 20 m in depth.
174 According to Figure 5, ground temperatures fluctuated seasonally at above 20 m in depth. However,
175 seasonal variations in ground temperature dwindled gradually below 30 m (Figure 6), leaving only inter-

176 annual variations. Ground temperatures in Borehole GH4 increased with increasing depth (−2.51, −1.76
177 and −0.41 °C at 30, 50 and 80 m, respectively), whereas the thermal fluctuations declined downwards
178 (0.2 °C at 20 and 30 m in depth, but 0.03 °C at 80 m). Thus, during 2012-2020, the ground at depths of
179 30-80 m at the GH4 site was warming at an average rate of 0.04-0.20 °C /dec.

180 In Borehole YTLH2, remarkable seasonal variations were noted at each measured depth. The seasonal
181 amplitude of ground temperature gradually dampened with increasing depth, varying from approximately
182 0.5 °C at 8 m in depth to less than 0.1 °C at 20 m. Unlike permafrost in Mangui town and Gen'he city, a
183 significant cooling of permafrost was detected at all depths except 20 m at YTLH2 during the 10-year
184 observation (Figure 7). The average rate of temperature change at 20 m depth is close to 0 °C /dec and
185 the MAGT here has been roughly maintained at −0.49 °C in the past decade (Table 2).

186 **4 Discussion**

187 **4.1 Change trends of near-surface permafrost temperatures**

188 Based on the analysis in Section 3.1, it can be inferred that changes in the ground thermal regimes of the
189 ecosystem-dominated permafrost on the northwestern slope of the Da Xing'anling Mountains are mainly
190 controlled by changes in local factors, such as vegetation and snow covers and human activities,
191 especially in the ALT. For example, ALT ranges from 2.5 m in 2016 and 2017 to 1.9 m in 2020 for the
192 site in shrubs (MG1), 4.8 m in 2017 to 4.2 m in 2020 in sedge meadow (MG2) and 2.9 m in 2012 to 4.0
193 m in 2014 in the farmer's backyard (MG3) during the observation period. Apparently, the Borehole MG1,
194 far away from downtown Mangui, had the least ALT because of more shading effect of shrubs than that
195 of meadow (MG2) and less anthropogenic impact than that of backyard (MG3). Declining trend of ALT
196 was also observed in the Nanwenghe Wetlands Reserve on the southern slope of the Da Xing'anling-
197 Yile'huli Mountain Knots, Northeast China, probably driven by a rising surface and thermal offsets of
198 vegetation cover and organic soils (He et al., 2021). Additionally, at the MG3 site, the smaller ALT could
199 be attributed to the shading effect of the farmer's house and more heat loss to the atmosphere caused by
200 snow removal in the yard in winter as well. In Gen'he, at the site of Borehole GH4 in a primeval forest,
201 ALT remained unchanged at 2.2 m from 2012 to 2016 and, without human disturbance, permafrost was
202 well-preserved. On the contrary, at the GH5 site in the suburb meadow frequently disturbed by the nearby
203 livestock, a complex thermal regime was observed in the active layer. Ground temperatures at the depths

204 of 3.5-6.0 m were negative from March to September and positive in other time every year, and; not until
205 7.0 m in depth, where it became below 0° C all the year round. By definition, the active layer is the layer
206 above permafrost that freezes in winter and thaws in summer. Therefore, 7 m is supposed to be the
207 reasonable ALT or the depth of the permafrost table, and there might be no supra-permafrost subaerial
208 talik (Jin et al., 2021) between the active layer and the permafrost table at this site, i.e., attached
209 permafrost. However, the supra-permafrost subaerial talik, which has appeared in the Nanwenghe
210 Wetlands Reserve about 300 km to the east of the study site (He et al., 2021), may develop at this site in
211 the future. In Yituli'he, the two boreholes (YTLH1 and YTLH2) are, about 20 m apart, both in the
212 meadowy swamp to the east of the railway and to the west of highway. Permafrost here is well developed,
213 partially thanks to the sufficient moisture provided by lowland swamp, which also possibly facilitates
214 the formation of ice wedges (Yang and Jin, 2011).

215 Notably, there was a decreasing trend in ground temperatures at shallow depths no matter in summer or
216 winter during 2010-2020 (Figure 2), otherwise suggesting a cooling permafrost at shallow depths in the
217 last decade on the northwestern slope of the Da Xing'anling Mountains if no ground-surface conditions
218 are taken into account. The maximum thaw depth (MTD) in Yituli'he rose gradually with fluctuations
219 during 1980-2005, and it showed a downward trend during 2010-2019 (Figure 8). This could be related
220 to the thriving vegetation, and declining winter precipitation or snow cover in this area during the
221 observational period. In the last decade, although the mean positive air temperature (MPAT) barely
222 changed in Gen'he (Fig 9b), precipitation in warm seasons increased slightly, leading to a wetter
223 condition in favor of vegetation thriving. For example, the maximum vegetation height of *Carex tato* at
224 YTLH1 and YTLH2 grew significantly from 2009 to 2014. Bushes have also emerged recently near the
225 borehole. Thriving vegetation will reduce the solar irradiance incident onto the soil surface in summer
226 and cast a cooling effect on the ground temperature. On the contrary, the winter precipitation (Figure 9a)
227 and snow cover, including the maximal snow depth (Figure 9c) and snow duration (Figure 9d), declined
228 slightly. The thermal insulation effect of snow cover will be weakened when the snow the depth of snow
229 cover decreased, which will lead to a larger heat removal from the permafrost to air in winter and drive
230 the permafrost cooling. The detail mechanisms for the cooling permafrost will be further investigated
231 with the help of some physically based models after complementing observations on the interactions of
232 energy balance between the permafrost, vegetation, and snow cover.

233 4.2 Change trends of permafrost temperatures at larger depths

234 Permafrost in Mangui

235 During the observation period, the averages of MAGTs at the depth of 20 m were -0.79 , -0.70 and -0.93
236 $^{\circ}\text{C}$, respectively, in shrubs (MG1), meadow (MG2) and farmer's backyard, indicating a poor correlation
237 between the thermal state of deeper permafrost and vegetation cover or anthropic disturbances. However,
238 there was a close relationship between permafrost change at larger depths and land surface conditions.
239 Permafrost below 8 m was significantly warming in the last decade under a warming climate (Figure 4).
240 In Borehole-MG1 and Borehole-MG2 in particular, the rates of ground warming increased slightly with
241 depth (<0.3 $^{\circ}\text{C}/\text{dec}$ for MG1 and <0.2 $^{\circ}\text{C}/\text{dec}$ for MG2), demonstrating a less significant thermal rising
242 in deeper permafrost. Within the zone of discontinuous permafrost, the negative relationship between
243 effective leaf area index (LAI_e) and soil moisture may contribute to differential rates of permafrost thaw
244 (Baltzer et al., 2014). Therefore, more effective water uptake by shrubs than meadow results in lower
245 soil moisture, leading to a more rapid thaw of permafrost at the MG1 site than that at the MG2 site. The
246 warming rate of permafrost in Borehole MG3, with a large warming range, decreased with depth
247 (0.5 $^{\circ}\text{C}/\text{dec}$ at depths of 10 and 12 m, but approximately 0.2 $^{\circ}\text{C}/\text{dec}$ at depths of 16 and 20 m), probably
248 due to short monitoring period and less data. However, it does verify that, in Mangui, permafrost at
249 depths is warming or degrading in the last decade.

250 Permafrost in Gen'he

251 Indeed, there exists some long periods with missing data at GH4, and it is reluctant to make the trend
252 analysis with these missing data. However, at the surface layers, although the fluctuation of ground
253 temperature is relatively huge, the collected data has generally captured the maximal and minimal ground
254 temperature in years with observing data. Simply by a visual inspection, the minimal or maximal ground
255 temperature has an apparent warming trend from 2012 to 2020, which has a good coincidence with the
256 trend analysis in this study. That is, although the missing values could make some loss for the accuracy
257 of trending analysis, or make it less robust, they will not change the trend in an antipodal way. In addition,
258 in depths greater than 8 m, the annual fluctuation of ground temperature was much less than the surface
259 layers, as shown in Figure 5 and 6. The missing values will not vary too much from the collected values.
260 Therefore, we speculate the influence of missing values on trending analysis for deep layers will be
261 smaller than that in the surface layers, and it will decrease with depth, which can be inferred from Figure

262 5 and 6.

263 In Borehole GH4, lower ground temperatures and greater warming range was observed in comparison
264 with those in Borehole GH5 in the last decade (Figure 5). Even at depths of 70 and 80 m, ground
265 temperatures were still rising with time at appreciable warming rates (Figure 6), reflecting the impact of
266 climatic warming on permafrost at greater depths. A subtle warming trend of permafrost at depths of 8-
267 20 m in Borehole GH5 was also detected with a rate of 0.04 °C/dec during the observation period (Figure
268 5). This warming rate of ground temperature is similar to that of the Borehole 85-8A in the southern zone
269 of discontinuous permafrost in North America, where the permafrost is often vertically in isothermal
270 condition and close to 0 °C in ground temperature (Smith et al., 2010). In this situation, latent heat effects
271 are considered as the key factor for leading to isothermal conditions in the ground and allowing
272 permafrost to persist under a warming climate (Smith et al., 2010). If the effect of large thermal inertia
273 lasts long enough, the supra-permafrost subaerial talik will be highly likely to form and permafrost will
274 be gradually buried. In a word, permafrost degradation in Gen'he is also evident at present in both
275 forested landscape and anthropic zones, particularly in the latter one.

276 **Permafrost in Yituli'he**

277 According to previous study (Jin et al., 2007), MAGT at 13 m in Yituli'he rose by 0.2 °C during 1984-
278 1997, continuously rising from -1.00 °C in 1997 to -0.55 °C in 2010, except during the short suspension
279 of monitoring (2005-2008), and peaking at -0.53 °C in 2013. After that, it kept lowering consecutively
280 and by 2018 it was lower than -0.70 °C, showing an evident cooling trend of permafrost in a sharp
281 contrast to the ground warming trends in Gen'he, Mangui, and other permafrost regions in the world
282 (Douglas et al., 2021; Farquharson et al., 2019). Based on the investigation, there was once a Railway
283 Branch Administration in Yituli'he town since 1964s to 1970s, with a population of over 30,000, but the
284 branch was terminated in 1998. After that, more and more people emigrated and less than 10,000
285 residents have remained at present, thus leaving a chance for restoration of the local eco-environment
286 and for recovering permafrost temperature.

287 So far, the mitigation of permafrost degradation becomes considerably difficult in the context of a
288 persistent climate warming (Brown et al., 2015; Luo et al., 2018). However, within the dried margin of
289 the Twelvemile Lake (66°27'N, 145°34'W), permafrost aggradation has taken place due to willow shrub
290 uptake of summer recharge and summer shading recharge reduction (Briggs et al., 2014). Beer et al.

291 (Beer et al., 2020) also found that most permafrost-affected soil could be preserved by increasing the
292 population density of big herbivores in northern high-latitude ecosystems as a result of reducing
293 insulation of winter snow cover. The fact that permafrost is cooling in Yituli'he demonstrates that the
294 ecosystem-protected permafrost in discontinuous permafrost zone may recover if the disturbances, such
295 as human activities, dwindle. Thus, our research results would provide key evidence for the preservation
296 of permafrost in areas with intense past anthropic disturbances (Serban et al., 2021).

297 **5 Conclusions**

298 Long-term records of permafrost monitoring presented here from the northwestern flank of the Da
299 Xing'anling Mountains in Northeast China show some important characteristics of ground thermal
300 regimes in the past eight years (2012-2020). The lowest MAGT at 20 m in depth was -2.83 °C in
301 Borehole GH4 in a primeval larch forest, and -0.94 , -0.80 , -0.70 , -0.60 and -0.49 °C, respectively, at
302 MG3, MG1, MG2, GH5 and YTLH2. The maximum of the burial depth of the permafrost table at about
303 7.0 m was discovered in Borehole GH5, and the minimum, 1.1 ~ 1.5 m at YTLH1. The permafrost table
304 was at depths of about 2.0 m at GH4 and YTLH2, and 2.5, 5.0 and 4.0 m at MG1, MG2 and MG3,
305 respectively. Local factors, such as vegetation and snow covers and human activities, are supposed to be
306 mainly responsible for the changes in the ALT and the thermal state of shallow permafrost in the study
307 area. The most important fact is that ground cooling at shallow depths, as well as the declining ALT in
308 Yituli'he after 2009, has been detected during the observation period, which is probably caused by fairly
309 constant MPAT (mean positive air temperature) and weakened insulation of winter snow cover.

310 Apart from Yituli'he, permafrost warming at large depths was particularly pronounced during the
311 observation period, even at depths of 70 and 80 m, with different ground warming rates. It is noteworthy
312 that geothermal gradient at depths in Borehole GH5 is almost zero (vertically no change) and with MAGT
313 at about 0 °C due to huge thermal inertia of the ice-rich permafrost. This may most likely lead to the
314 formation of the supra-permafrost subaerial talik soon. At the Yituli'he Permafrost Observatory,
315 permafrost has been cooling since the re-establishment of monitoring program in 2010; the rapidly
316 declining local population might have relieved its stress on the eco-environment and resulted in
317 permafrost recovery. This fact makes it possible to mitigate the permafrost degradation in the zone of
318 ecosystem-dominated permafrost, offering a new thought for permafrost protection.

319 **Author Contributions**

320 XC, HJ, and RH designed the study. XC wrote the manuscript and performed the analysis. YZ
321 plotted the figures. XL, XJ and GL contributed parts of the field data. HJ improved the writing and
322 structure of the paper.

323 **Competing interests**

324 The contact author has declared that neither they nor their co-authors have any competing interests.

325 **Disclaimer**

326 Publisher's note: Copernicus Publications remains neutral with regard to jurisdictional claims in
327 published maps and institutional affiliations.

328 **Special issue statement**

329 This article is part of the special issue "Extreme environment datasets for the three poles". It is not
330 associated with a conference.

331 **Acknowledgements**

332 Thanks go to the Inner Mongolia Agricultural University for fieldwork support and the Gen'he Weather
333 Bureau for meteorological data provision. This study was financially supported by the National Natural
334 Science Foundation of China (Grant Nos. 41971079, 41671059, 41871052 and U20A2082) and the
335 Natural Science Program of Hunan Province (Grant No. 2020JJ5161).

336 **Data availability**

337 The dataset is available from the National Tibetan Plateau/Third Pole Environment Data Center
338 (<https://doi.org/10.11888/Geocry.tpdc.271752>, Chang X, 2021).

339 **Reference**

340 Ala-Aho, P., Autio, A., Bhattacharjee, J., Isokangas, E., Kujala, K., Marttila, H., Menberu, M., Meriö, L.
341 J., Postila, H., Rauhala, A., Ronkanen, A. K., Rossi, P. M., Saari, M., Haghghi, A. T., and Kløve, B.:
342 What conditions favor the influence of seasonally frozen ground on hydrological partitioning? A
343 systematic review, *Environmental Research Letters*, 16, 043008, 10.1088/1748-9326/abe82c, 2021.
344 Baltzer, J. L., Veness, T., Chasmer, L. E., Sniderhan, A. E., and Quinton, W. L.: Forests on thawing
345 permafrost: fragmentation, edge effects, and net forest loss, *Global change biology*, 20, 824-834,
346 10.1111/gcb.12349, 2014.
347 Beer, C., Zimov, N., Olofsson, J., Porada, P., and Zimov, S.: Protection of Permafrost Soils from Thawing
348 by Increasing Herbivore Density, *Scientific reports*, 10, 4170, 10.1038/s41598-020-60938-y, 2020.

349 Biskaborn, B. K., Smith, S. L., Noetzli, J., Matthes, H., Vieira, G., Streletskiy, D. A., Schoeneich, P.,
350 Romanovsky, V. E., Lewkowicz, A. G., Abramov, A., Allard, M., Boike, J., Cable, W. L., Christiansen,
351 H. H., Delaloye, R., Diekmann, B., Drozdov, D., Etzelmüller, B., Grosse, G., Guglielmin, M., Ingeman-
352 Nielsen, T., Isaksen, K., Ishikawa, M., Johansson, M., Johannsson, H., Joo, A., Kaverin, D., Kholodov,
353 A., Konstantinov, P., Kröger, T., Lambiel, C., Lanckman, J.-P., Luo, D., Malkova, G., Meiklejohn, I.,
354 Moskalenko, N., Oliva, M., Phillips, M., Ramos, M., Sannel, A. B. K., Sergeev, D., Seybold, C.,
355 Skryabin, P., Vasiliev, A., Wu, Q., Yoshikawa, K., Zheleznyak, M., and Lantuit, H.: Permafrost is
356 warming at a global scale, *Nature Communications*, 10, 264, 10.1038/s41467-018-08240-4, 2019.

357 Briggs, M. A., Walvoord, M. A., McKenzie, J. M., Voss, C. I., Day-Lewis, F. D., and Lane, J. W.: New
358 permafrost is forming around shrinking Arctic lakes, but will it last?, *Geophysical Research Letters*,
359 41, 1585-1592, <https://doi.org/10.1002/2014GL059251>, 2014.

360 Brown, D. R. N., Jorgenson, M. T., Douglas, T. A., Romanovsky, V. E., Kielland, K., Hiemstra, C.,
361 Euskirchen, E. S., and Ruess, R. W.: Interactive effects of wildfire and climate on permafrost
362 degradation in Alaskan lowland forests, *Journal of Geophysical Research: Biogeosciences*, 120, 1619-
363 1637, <https://doi.org/10.1002/2015JG003033>, 2015.

364 Brown, J., Hinkel, K. M., and Nelson, F. E.: The circumpolar active layer monitoring (calm) program:
365 Research designs and initial results, *Polar Geography*, 24, 166-258, 10.1080/10889370009377698,
366 2000.

367 Cao, B., Zhang, T., Wu, Q., Sheng, Y., Zhao, L., and Zou, D.: Permafrost zonation index map and
368 statistics over the Qinghai-Tibet Plateau based on field evidence, *Permafrost and Periglacial Processes*,
369 30, 178-194, 10.1002/ppp.2006, 2019.

370 Cao, B., Zhang, T., Peng, X., Mu, C., Wang, Q., Zheng, L., Wang, K., and Zhong, X.: Thermal
371 Characteristics and Recent Changes of Permafrost in the Upper Reaches of the Heihe River Basin,
372 Western China, *Journal of Geophysical Research: Atmospheres*, 123, 7935-7949,
373 <https://doi.org/10.1029/2018JD028442>, 2018.

374 Chen, S.-S., Zang, S., and Sun, L.: Characteristics of permafrost degradation in Northeast China and its
375 ecological effects: A review, *Sciences in Cold and Arid Regions*, 12, 1-11,
376 10.3724/sp.j.1226.2020.00001., 2020.

377 Douglas, T. A., Hiemstra, C. A., Anderson, J. E., Barbato, R. A., Bjella, K. L., Deeb, E. J., Gelvin, A. B.,
378 Nelsen, P. E., Newman, S. D., Saari, S. P., and Wagner, A. M.: Recent degradation of interior Alaska
379 permafrost mapped with ground surveys, geophysics, deep drilling, and repeat airborne lidar, *The*
380 *Cryosphere*, 15, 3555-3575, 10.5194/tc-15-3555-2021, 2021.

381 Everdingen, R. O. v.: Multi-language glossary of permafrost and related ground-ice terms, National Snow
382 and Ice Data Centre, Boulder, CO1998 (revised 2005).

383 Farquharson, L. M., Romanovsky, V. E., Cable, W. L., Walker, D. A., Kokelj, S. V., and Nicolsky, D.:
384 Climate Change Drives Widespread and Rapid Thermokarst Development in Very Cold Permafrost in
385 the Canadian High Arctic, *Geophysical Research Letters*, 46, 6681-6689,
386 <https://doi.org/10.1029/2019GL082187>, 2019.

387 Grebenets, V. I., Tolmanov, V. A., and Streletskiy, D. A.: Active Layer Dynamics Near Norilsk, Taimyr
388 Peninsula, Russia, *Geography, Environment, Sustainability*, 14, 55-66, 10.24057/2071-9388-2021-073,
389 2021.

390 Gruber, S.: Derivation and analysis of a high-resolution estimate of global permafrost zonation, *The*
391 *Cryosphere*, 6, 10.5194/tc-6-221-2012, 2012.

392 Guglielmin, M.: Ground surface temperature (GST), active layer and permafrost monitoring in

393 continental Antarctica, Permafrost and Periglacial Processes, 17, 133-143,
394 <https://doi.org/10.1002/ppp.553>, 2006.

395 Guglielmin, M., Worland, M. R., and Cannone, N.: Spatial and temporal variability of ground surface
396 temperature and active layer thickness at the margin of maritime Antarctica, Signy Island,
397 Geomorphology, 155-156, 20-33, <https://doi.org/10.1016/j.geomorph.2011.12.016>, 2012.

398 Guo, W., Liu, H., Anenkhonov, O. A., Shangguan, H., Sandanov, D. V., Korolyuk, A. Y., Hu, G., and Wu,
399 X.: Vegetation can strongly regulate permafrost degradation at its southern edge through changing
400 surface freeze-thaw processes, Agricultural and Forest Meteorology, 252, 10-17,
401 <https://doi.org/10.1016/j.agrformet.2018.01.010>, 2018.

402 He, R.-X., Jin, H.-J., Luo, D.-L., Li, X.-Y., Zhou, C.-F., Jia, N., Jin, X.-Y., Li, X.-Y., Che, T., Yang, X.,
403 Wang, L.-Z., Li, W.-H., Wei, C.-L., Chang, X.-L., and Yu, S.-P.: Permafrost changes in the Nanwenghe
404 Wetlands Reserve on the southern slope of the Da Xing'anling–Yile'huli mountains, Northeast China,
405 Advances in Climate Change Research, 12, 696-709, <https://doi.org/10.1016/j.accre.2021.06.007>, 2021.

406 Hrbáček, F., Vieira, G., Oliva, M., Balks, M., Guglielmin, M., de Pablo, M. Á., Molina, A., Ramos, M.,
407 Goyanes, G., Meiklejohn, I., Abramov, A., Demidov, N., Fedorov-Davydov, D., Lupachev, A., Rivkina,
408 E., Láska, K., Kňázková, M., Nývlt, D., Raffi, R., Strelin, J., Sone, T., Fukui, K., Dolgikh, A.,
409 Zazovskaya, E., Mergelov, N., Osokin, N., and Miamin, V.: Active layer monitoring in Antarctica: an
410 overview of results from 2006 to 2015, Polar Geography, 44, 217-231,
411 10.1080/1088937X.2017.1420105, 2021.

412 Jin, H., Wu, Q., and Romanovsky, V.: Degrading permafrost and its impacts, Advances in Climate
413 Change Research, 12, 10.1016/j.accre.2021.01.007, 2021.

414 Jin, H., Li, S., Cheng, G., Shaoling, W., and Li, X.: Permafrost and climatic change in China, Global and
415 Planetary Change, 26, 387-404, [https://doi.org/10.1016/S0921-8181\(00\)00051-5](https://doi.org/10.1016/S0921-8181(00)00051-5), 2000.

416 Jin, H., Yu, Q., Lü, L., Guo, D., He, R., Yu, S.-p., Sun, G., and Li, Y.: Degradation of permafrost in the
417 Xing'anling Mountains, northeastern China, Permafrost and Periglacial Processes, 18, 245-258, 2007.

418 Li, X.-Y., Jin, H.-J., Wang, H.-W., Marchenko, S. S., Shan, W., Luo, D.-L., He, R.-X., Spektor, V., Huang,
419 Y.-D., Li, X.-Y., and Jia, N.: Influences of forest fires on the permafrost environment: A review,
420 Advances in Climate Change Research, 12, 48-65, <https://doi.org/10.1016/j.accre.2021.01.001>, 2021.

421 Li, X., Jin, H., He, R., Huang, Y., Wang, H., Luo, D., Jin, X., Lü, L., Wang, L., Li, W. h., Wei, C., Chang,
422 X., Yang, S., and Yu, S.: Effects of forest fires on the permafrost environment in the northern Da
423 Xing'anling (Hinggan) mountains, Northeast China, Permafrost and Periglacial Processes, 30, 163-177,
424 <https://doi.org/10.1002/ppp.2001>, 2019.

425 Luo, L., Ma, W., Zhuang, Y., Zhang, Y., Yi, S., Xu, J., Long, Y., Ma, D., and Zhang, Z.: The impacts of
426 climate change and human activities on alpine vegetation and permafrost in the Qinghai-Tibet
427 Engineering Corridor, Ecological Indicators, 93, 24-35, <https://doi.org/10.1016/j.ecolind.2018.04.067>,
428 2018.

429 Mu, C., Abbott, B. W., Norris, A. J., Mu, M., Fan, C., Chen, X., Jia, L., Yang, R., Zhang, T., Wang, K.,
430 Peng, X., Wu, Q., Guggenberger, G., and Wu, X.: The status and stability of permafrost carbon on the
431 Tibetan Plateau, Earth-Science Reviews, 211, 103433, 10.1016/j.earscirev.2020.103433, 2020.

432 Ran, Y., Li, X., and Cheng, G.: Climate warming over the past half century has led to thermal degradation
433 of permafrost on the Qinghai–Tibet Plateau, The Cryosphere, 12, 595-608, 10.5194/tc-12-595-2018,
434 2018.

435 Ran, Y., Li, X., Cheng, G., Che, J., Aalto, J., Karjalainen, O., Hjort, J., Luoto, M., Jin, H., Obu, J., Hori,
436 M., Yu, Q., and Chang, X.: New high-resolution estimates of the permafrost thermal state and

437 hydrothermal conditions over the Northern Hemisphere, *Earth Syst. Sci. Data*, 14, 865-884,
438 10.5194/essd-14-865-2022, 2022.

439 Romanovsky, V. E., Smith, S. L., and Christiansen, H. H.: Permafrost thermal state in the polar Northern
440 Hemisphere during the international polar year 2007–2009: a synthesis, *Permafrost and Periglacial*
441 *Processes*, 21, 106-116, <https://doi.org/10.1002/ppp.689>, 2010.

442 Schuur, E. A. G. and Mack, M. C.: Ecological Response to Permafrost Thaw and Consequences for Local
443 and Global Ecosystem Services, *Annual Review of Ecology, Evolution, and Systematics*, 49, 279-301,
444 10.1146/annurev-ecolsys-121415-032349, 2018.

445 Schuur, E. A. G., McGuire, A. D., Schädel, C., Grosse, G., Harden, J. W., Hayes, D. J., Hugelius, G.,
446 Koven, C. D., Kuhry, P., Lawrence, D. M., Natali, S. M., Olefeldt, D., Romanovsky, V. E., Schaefer,
447 K., Turetsky, M. R., Treat, C. C., and Vonk, J. E.: Climate change and the permafrost carbon feedback,
448 *Nature*, 520, 171-179, 10.1038/nature14338, 2015.

449 Serban, R., Serban, M., He, R., Jin, H., Yan, L., Xinyu, L., Wang, X., and Li, G.: 46-Year (1973–2019)
450 Permafrost Landscape Changes in the Holo Basin, Northeast China Using Machine Learning and
451 Object-Oriented Classification, *Remote Sensing*, 13, 1910, 10.3390/rs13101910, 2021.

452 Shiklomanov, N., Streletskiy, D., and Nelson, F.: Northern Hemisphere Component of the Global
453 Circumpolar Active Layer Monitoring (CALM) Program, 2012.

454 Shur, Y. and Jorgenson, M.: Patterns of Permafrost Formation and Degradation in Relation to Climate
455 and Ecosystems, *Permafrost and Periglacial Processes*, 18, 7-19, 10.1002/ppp.582, 2007.

456 Sim, T. G., Swindles, G. T., Morris, P. J., Baird, A. J., Cooper, C. L., Gallego-Sala, A. V., Charman, D.
457 J., Roland, T. P., Borken, W., Mullan, D. J., Aquino-López, M. A., and Galka, M.: Divergent responses
458 of permafrost peatlands to recent climate change, *Environmental Research Letters*, 16, 034001,
459 10.1088/1748-9326/abe00b, 2021.

460 Smith, S. L., Romanovsky, V. E., Lewkowicz, A. G., Burn, C. R., Allard, M., Clow, G. D., Yoshikawa,
461 K., and Throop, J.: Thermal state of permafrost in North America: a contribution to the international
462 polar year, *Permafrost and Periglacial Processes*, 21, 117-135, <https://doi.org/10.1002/ppp.690>, 2010.

463 Wei, Z., Jin, H., Zhang, J., Yu, S., Han, X., Ji, Y., He, R., and Chang, X.: Prediction of permafrost changes
464 in Northeastern China under a changing climate, *Science China Earth Sciences*, 54, 924-935,
465 10.1007/s11430-010-4109-6, 2011.

466 Yang, S. and Jin, H.: $\delta^{18}O$ and δD records of inactive ice wedge in Yitulihe, Northeastern China and
467 their paleoclimatic implications, *Science China Earth Sciences*, 54, 119-126, 10.1007/s11430-010-
468 4029-5, 2011.

469 Zhang, G., Nan, Z., Wu, X., Ji, H., and Zhao, S.: The Role of Winter Warming in Permafrost Change
470 Over the Qinghai-Tibet Plateau, *Geophysical Research Letters*, 46, 11261-11269,
471 <https://doi.org/10.1029/2019GL084292>, 2019.

472 Zhang, T., Nelson, F., and Gruber, S.: Introduction to special section: Permafrost and Seasonally Frozen
473 Ground Under a Changing Climate, *Journal of Geophysical Research*, 112, 10.1029/2007JF000821,
474 2007.

475 Zhang, Y., Cheng, G., Jin, H., Yang, D., Flerchinger, G., Chang, X., Wang, X., and Liang, J.: Influences
476 of Topographic Shadows on the Thermal and Hydrological Processes in a Cold Region Mountainous
477 Watershed in Northwest China, *Journal of Advances in Modeling Earth Systems*, 10,
478 10.1029/2017MS001264, 2018a.

479 Zhang, Y., Cheng, G., Jin, H., Yang, D., Flerchinger, G., Chang, X., Bense, V., Han, X., and Liang, J.:
480 Influences of frozen ground and climate change on the hydrological processes in an alpine watershed:

481 A case study in the upstream area of the Hei'he River, Northwest China, Permafrost and Periglacial
 482 Processes, 28, 420-432, 2017.

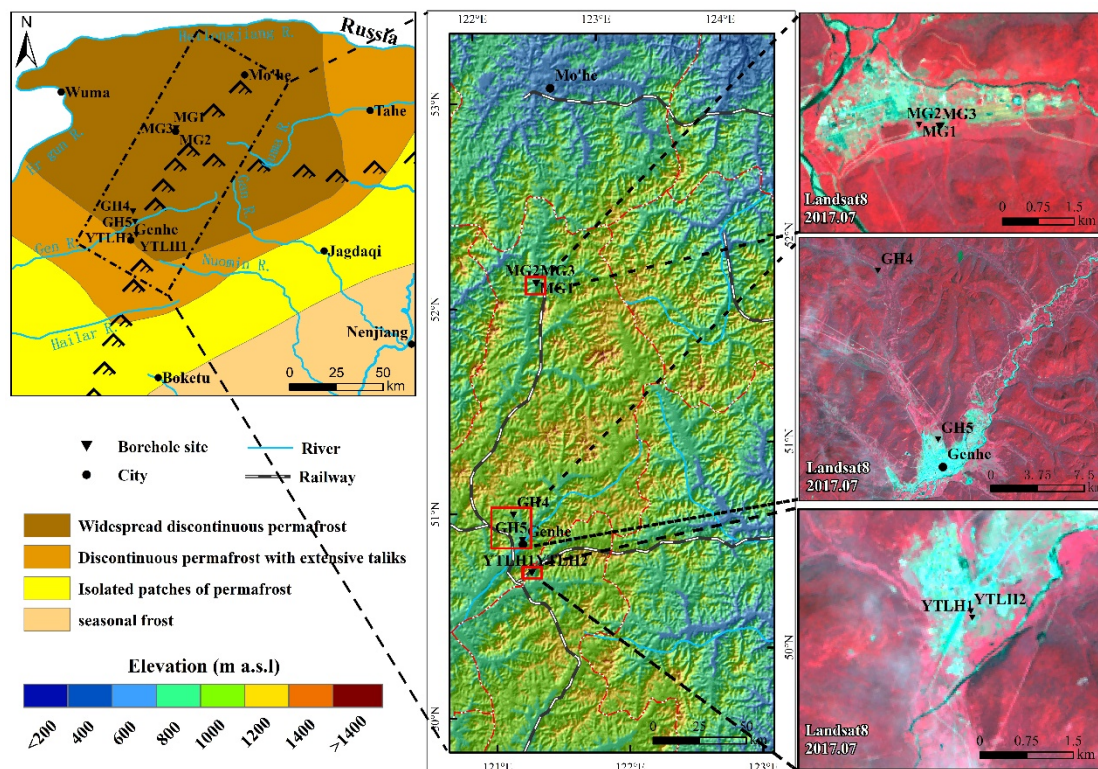
483 Zhang, Z.-Q., Wu, Q.-B., Hou, M.-T., Tai, B.-W., and An, Y.-K.: Permafrost change in Northeast China
 484 in the 1950s–2010s, Advances in Climate Change Research, 12, 18-28,
 485 <https://doi.org/10.1016/j.accre.2021.01.006>, 2021.

486 Zhang, Z., Wu, Q., Xun, X., Wang, B., and Wang, X.: Climate change and the distribution of frozen soil
 487 in 1980–2010 in northern northeast China, Quaternary International, 467, 230-241,
 488 <https://doi.org/10.1016/j.quaint.2018.01.015>, 2018b.

489 Zou, D., Zhao, L., Sheng, Y., Chen, J., Hu, G., Wu, T., Wu, J., Xie, C., Wu, X., Pang, Q., Wang, W., Du,
 490 E., Li, W., Liu, G., Li, J., Qin, Y., Qiao, Y., Wang, Z., Shi, J., and Cheng, G.: A new map of permafrost
 491 distribution on the Tibetan Plateau, The Cryosphere, 11, 2527-2542, 10.5194/tc-11-2527-2017, 2017.

492

493



494
 495 **Figure 1. Location of the study area and the distribution of Mangui1 (MG1), Mangui2 (MG2), Mangui3**
 496 **(MG3), Gen'he4 (GH4), Gen'he5 (GH5), Yituli'he1 (YTLH1) and Yituli'he2 (YTLH2) in the zones of frozen**
 497 **ground in the northern Da Xing'anling Mountains, Northeast China (The permafrost distribution is from**
 498 **Jin et al. (2007).)**
 499

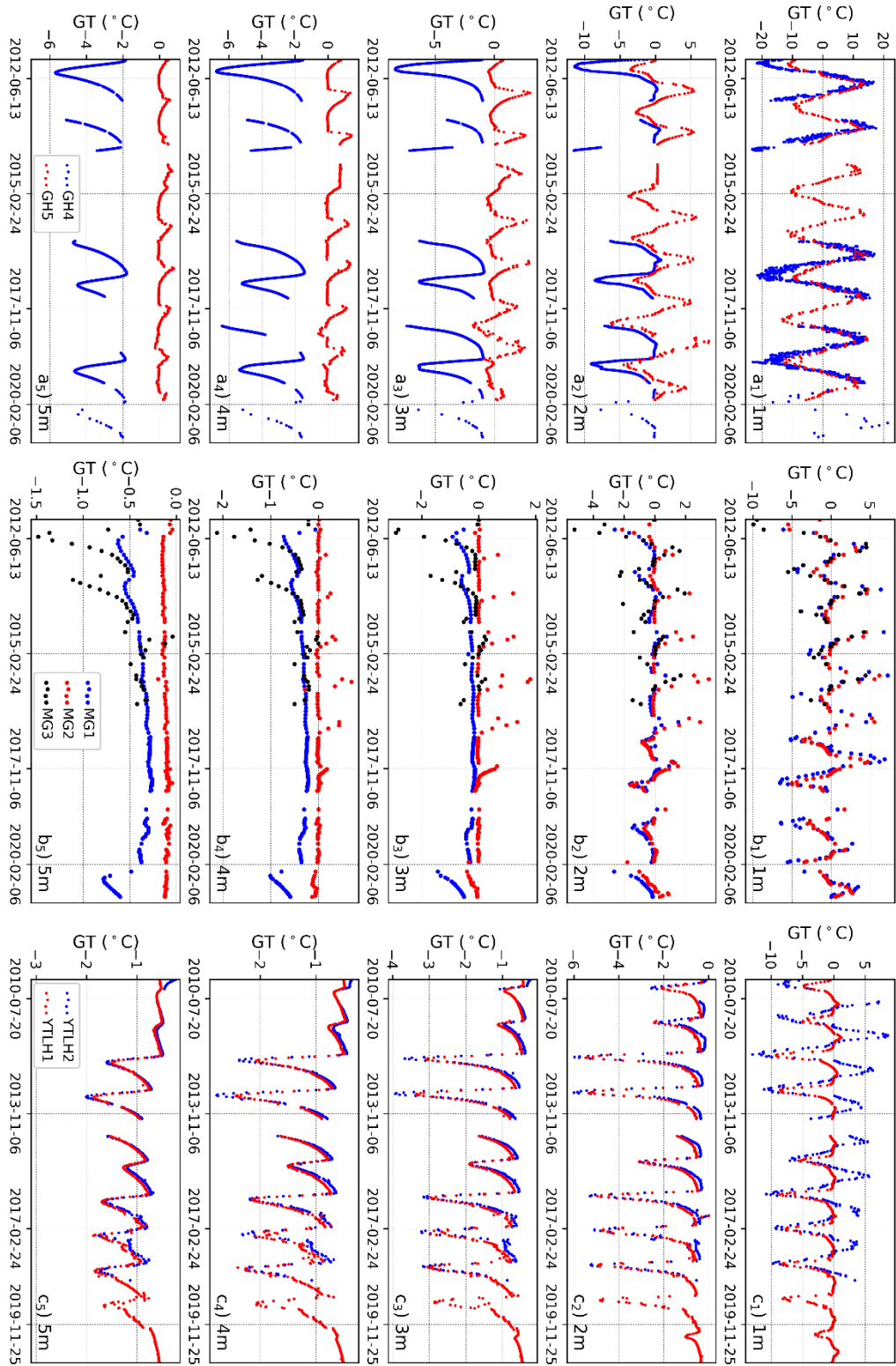


Figure 2. Variability of measured ground temperatures at depths of 1-5 m for Boreholes GH4 and GH5 (a), MG1, MG2 and MG3 (b), and YTLH1 and YTLH2 (c).

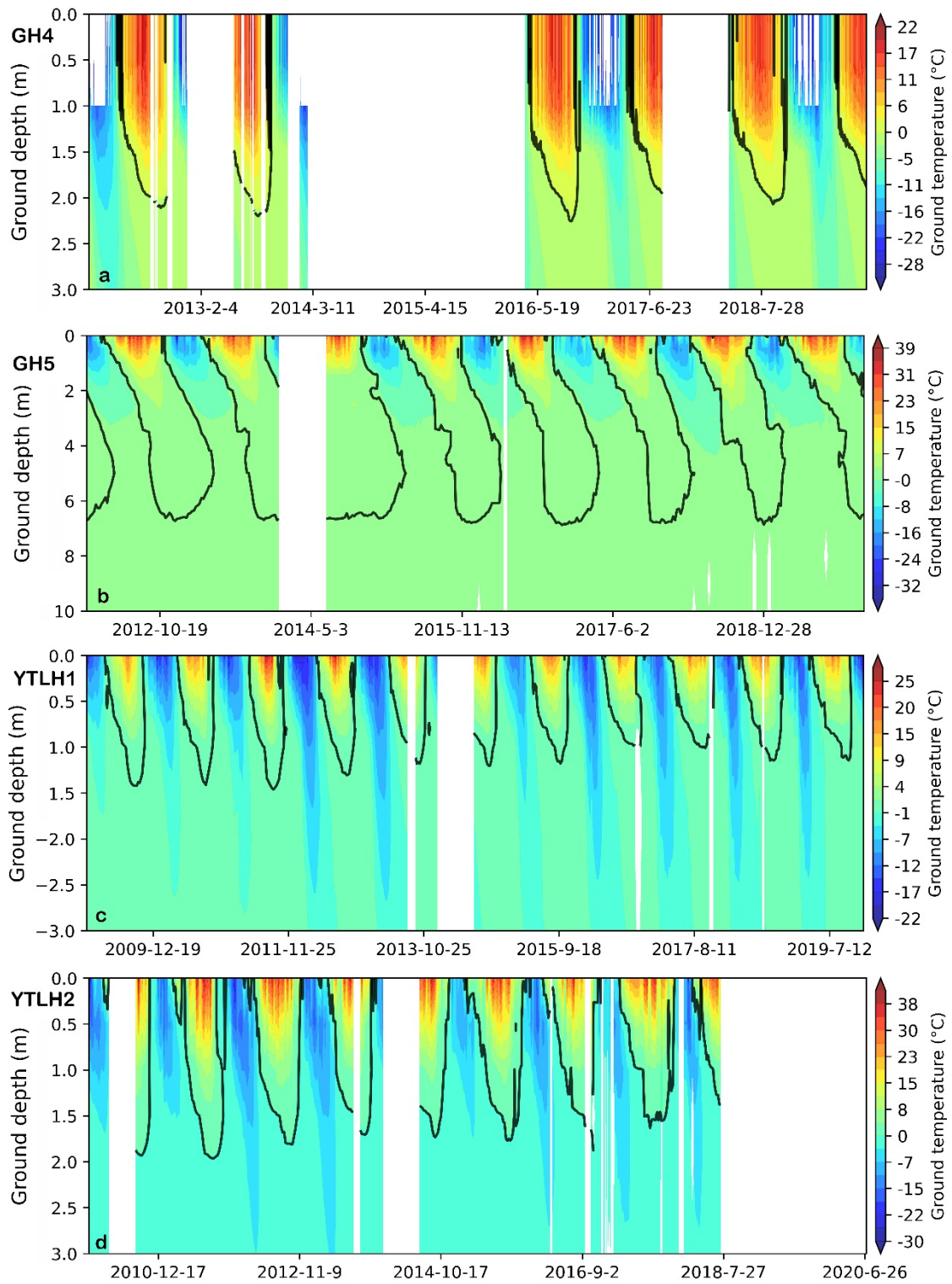


Figure 3 Variability of 0 °C isotherms (black curves) of ground temperature for Boreholes GH4 (a), GH5 (b), YTLH1 (c), and YTLH2 (d). The empty space indicates the period of missing data.

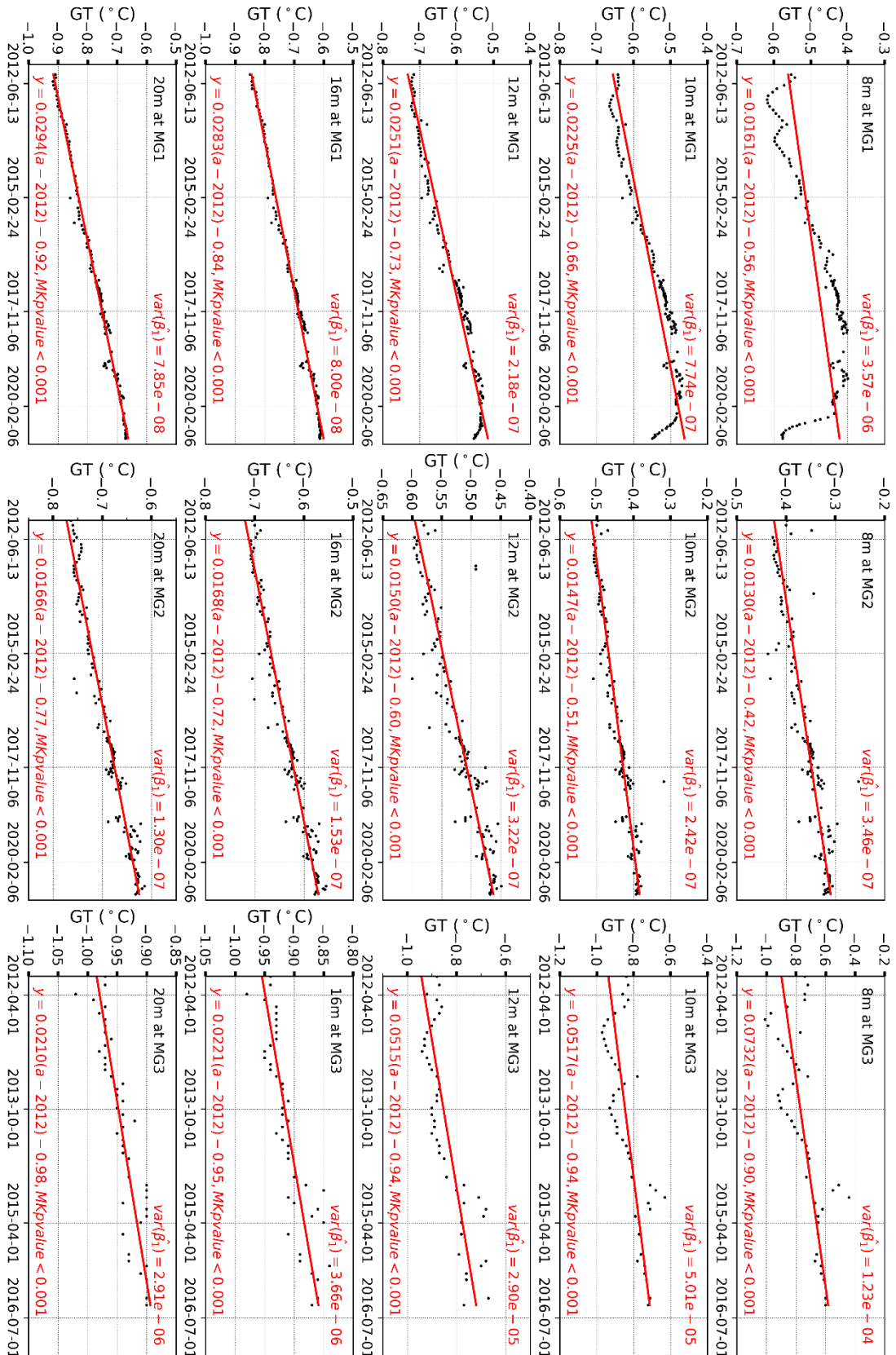


Figure 4. Variability of permafrost temperatures at depths of 8, 10, 12, 16 and 20 m in Boreholes MG1, MG2 and MG3 in Mangui, northern Da Xing'anling Mountains, Northeast China during 2012-2020. GT stands for ground temperature.

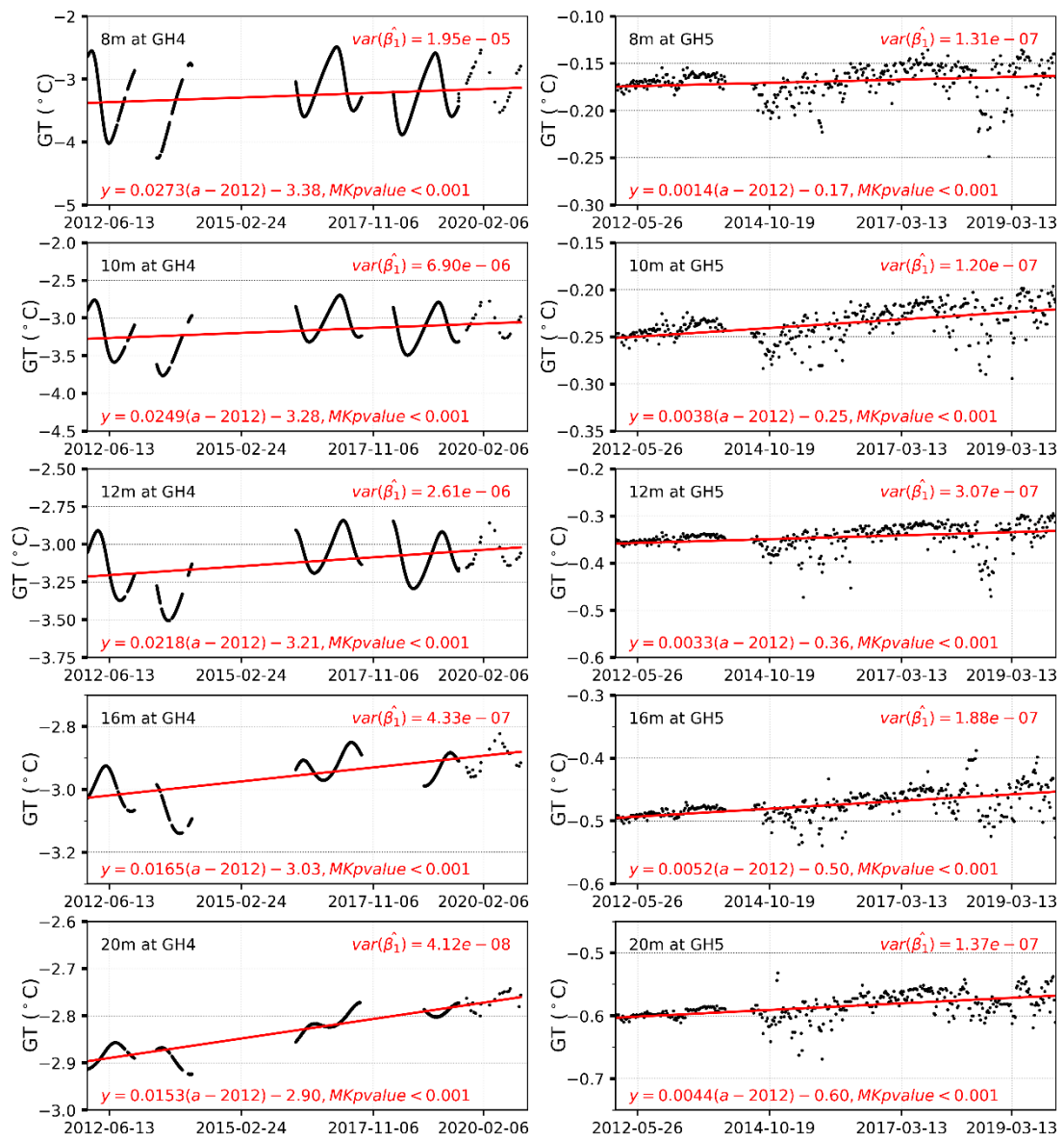


Figure 5. Variations in permafrost temperatures at depths of 8, 10, 12, 16 and 20 m in Boreholes GH4 and GH5 in Gen'he, northern Da Xing'anling Mountains, Northeast China during 2012-2020. GT stands for ground temperature.

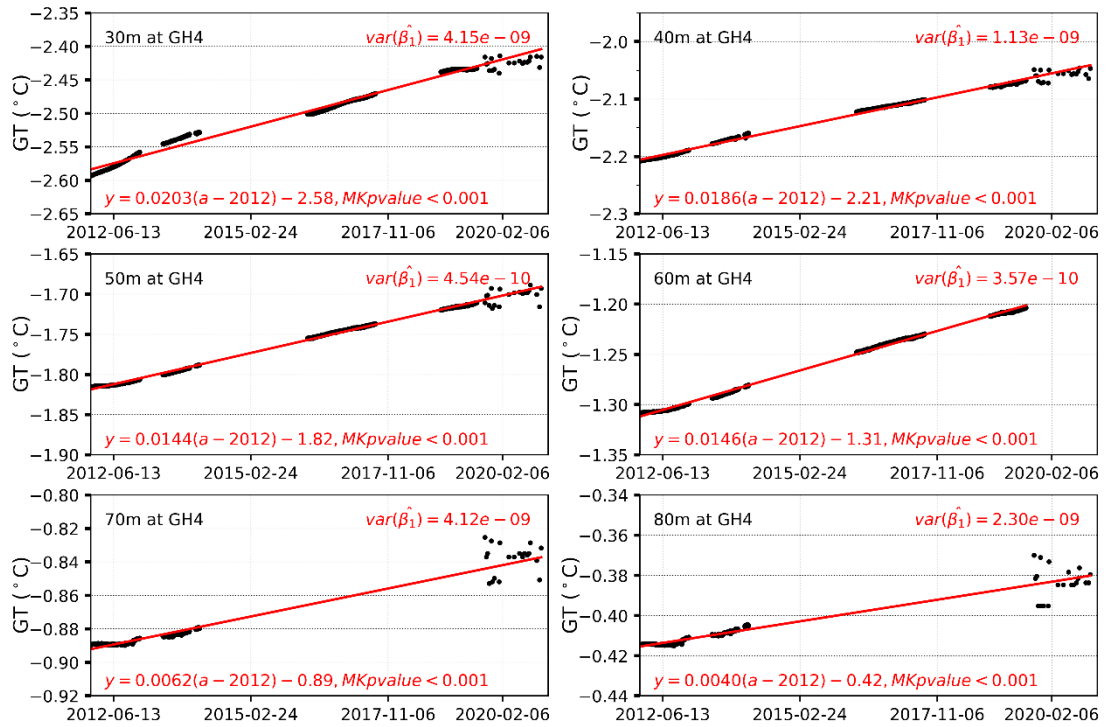


Figure 6. Variability of deep permafrost temperatures at depths of 30 – 80 m for Borehole GH4 in Gen’he, northern Da Xing’anling Mountains, Northeast China during 2012-2020. GT stands for ground temperature.

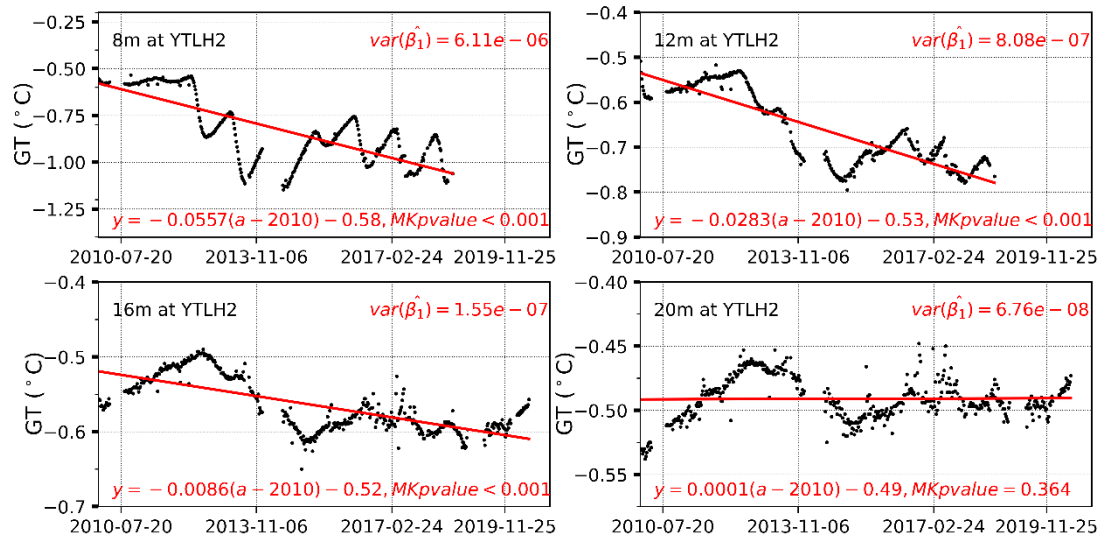


Figure 7. Variability of permafrost temperatures at depths of 8, 12, 16 and 20 m at Borehole YTLH2 in Yituli’he in northern Da Xing’anling Mountains, Northeast China during 2012-2020. GT stands for ground temperature.

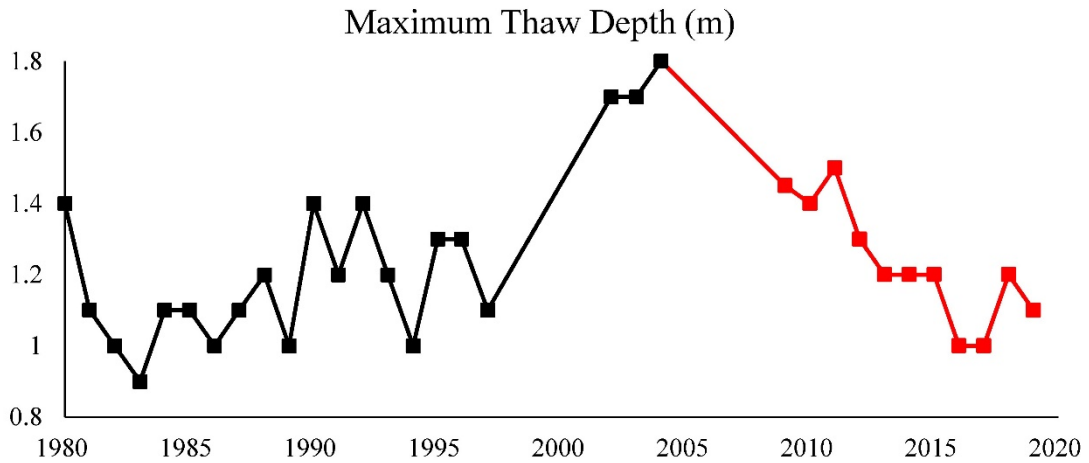


Figure 8. The maximum thaw depth (1980-2019) in Yituli'he on the northwestern flank of the northern Da Xing'anling Mountains in Northeast China (Black squares appeared in the paper from Jin et al. (2007), red ones are obtained in this observation. The two boreholes are 10 m from each other, with similar surface, hydrology and soil conditions.)

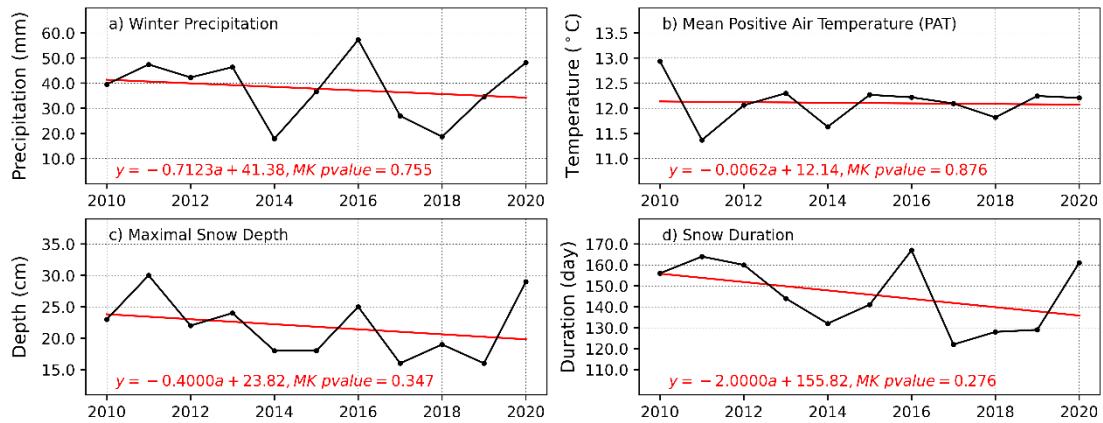


Figure 9. Climatic characteristics of Gen'he on the northwestern flank of the northern Da Xing'anling Mountains in Northeast China in the past ten years

Table 1. Characteristics and monitoring information of ground temperature boreholes in the northwestern part of Da Xing'anling Mountains, Northeastern China

Borehole No.	Lat. (°N)	Long. (°E)	Elev. (m a. s. l.)	Vegetation	Monitoring depths (m)	Time period	Monitoring frequency
MG1	52.037	122.069	633	<i>Betula fruticosa</i> shrubs	0.0, 1.0, 1.5, 2.0, 2.5, 3.0, 3.5, 4.0, 4.5,	2012-2020	Monthly
MG2	52.036	122.075	642	<i>Carex tato</i> meadow	5.0, 6.0, 7.0, 8.0, 9.0, 10.0, 11, 12, 13, 14, 15, 16, 17, 18, 19, 20	2012-2020	
MG3	52.036	122.076	639	Open courtyard		2012-2015	
GH4	50.932	121.502	811	<i>Betula fruticosa</i>	0.0, 1.0, 1.5, 2.0, 2.5, 3.0, 3.5, 4.0, 4.5,	2012-2014, 2016-2017,	Hourly
				<i>Larix gmelini</i> forest	5.0, 6.0, 7.0, 8.0, 9.0, 10.0, 11, 12, 13, 14, 15, 16, 17, 18, 19, 20, 25, 30, 35, 40, 45, 50, 60, 70, 80		
GH5	50.799	121.530	728	<i>Carex tato</i> meadow	0.0, 1.0, 1.5, 2.0, 2.5, 3.0, 3.5, 4.0, 4.5,	2012-2019	
				<i>Carex tato</i> swamp	5.0, 6.0, 7.0, 8.0, 9.0, 10.0, 11, 12, 13, 14, 15, 16, 17, 18, 19, 20		
YTLH1	50.629	121.549	721	<i>Carex tato</i> swamp	0.0, 0.1, 0.2, 0.5, 0.8, 1.0, 1.6, 2.0, 3.0, 4.0, 5.0, 6.0, 7.0, 8.15	2009-2019	Weekly
YTLH2	50.630	121.549	725	<i>Carex tato</i> swamp	0.0, 1.0, 1.5, 2.0, 2.5, 3.0, 3.5, 4.0, 4.5, 5.0, 6.0, 7.0, 8.0, 9.0, 10.0, 11, 12, 13, 14, 15, 16, 17, 18, 19, 20	2010-2017	

Table 2 ALT and average MAGTs of boreholes at larger depths in the northwestern Da Xing'anling Mountains, Northeast China

Borehole	ALT (m)	Average MAGT (°C)				
		8m	10m	13m	16m	20m
MG1	1.9-2.6	-0.48(ZAA)	-0.55	-0.63	-0.71	-0.77
MG2	4.3-4.8	-0.34(ZAA)	-0.44	-0.55	-0.63	-0.69
MG3	2.8-4.0	-0.75	-0.83	-0.87(ZAA)	-0.91	-0.94
GH4	2.0-2.2	-3.26	-3.17	-3.06	-2.96(ZAA)	-2.84
GH5	7.0	-0.17(ZAA)	-0.24	-0.39	-0.47	-0.59
YTLH2	1.5-2.0	-0.82	-0.74	-0.61(ZAA)	-0.56	-0.49